The Canadian Mineralogist
Vol. 42, pp. 1651-1666 (2004)

PREDICTION OF CRYSTAL MORPHOLOGY OF COMPLEX URANYL-SHEET MINERALS. II. OBSERVATIONS

MICHAEL SCHINDLER[§] AND ANDREAS MUTTER

Institut für Mineralogie, Universität Münster, Corrensstr. 24, D-48149 Münster, Germany

FRANK C. HAWTHORNE

Department of Geological Sciences, University of Manitoba, Winnipeg, Manitoba R3T 2N2, Canada

ANDREW PUTNIS

Institut für Mineralogie, Universität Münster, Corrensstr. 24, D-48149 Münster, Germany

ABSTRACT

The morphology of basal faces of uranyl-sheet minerals is predicted by considering the bond-valence deficiency of the chains of polyhedra, the shift between the layers, and the arrangement of the interstitial complexes between the layers. The sheet structural units of schoepite, $[(UO_2)_8O_2(OH)_{12}](H_2O)_{12}$, and fourmarierite, $Pb[(UO_2)_4O_3(OH)_4](H_2O)_4$, have the same underlying anion-topology. The stabilities of their edges differ because adjacent layers in schoepite are shifted by one chain of polyhedra, whereas adjacent layers are not shifted in fourmarierite. The minerals becquerelite, $^{[7]}Ca(H_2O)_4[(UO_2)_3O_2(OH)_3]_2\ (H_2O)_4$, compreignacite, $^{[7]}K_2(H_2O)_3\ [(UO_2)_3O_2(OH)_3]_2(H_2O)_4$, billietite, $^{[10]}Ba(H_2O)_4[(UO_2)_3O_2(OH)_3]_2\ (H_2O)_3$, protasite, $^{[10]}Ba(H_2O)_3[(UO_2)_3O_3(OH)_2]$, and masuyite, $^{[10]}Pb(H_2O)_3[(UO_2)_3O_3(OH)_2]$, all have structural units with the same basic anion-topology. The stabilities of their edges differ because of the different arrangements of interstitial species. In becquerelite, the interstitial cations are arranged in rows parallel to [010], whereas in billietite and compreignacite, the interstitial cations are arranged in rows parallel to [100]. For masuyite and protasite, the stability of their edges is defined by large differences in the bond-valence deficiencies of the chains of polyhedra with left and right terminations. The stabilities of edges in curite, $Pb_3[(UO_2)_8O_8(OH)_6](H_2O)_3$, are dictated by the low bond-valence deficiencies of the chains of polyhedra parallel to [001] and [011], and by the arrangement of cations in rows parallel to [001]. Minerals of the carnotite group contain the structural unit $[(UO_2)_2(V_2O_8)]^{2-}$, and the stability of the edges of their sheets is determined by the low bond-valence deficiency of chains of polyhedra parallel to [010 and [110]. Minerals of the uranophane group are based on the $[(UO_2)SiO_3(OH)]^-$ sheet, and the stabilities of their edges are more strongly affected by the bond-valence deficiency of the chains of polyhedra than by the arrangement of the interstitial cations, and by the shift in the sheets. All predictions are compared with the corresponding morphologies of crystals recorded by Atomic Force Microscopy (AFM), on images of crystals, and on crystal drawings from the (mainly older) mineralogical literature. All predictions are in good agreement with the observed morphology of the basal faces.

Keywords: uranyl minerals, morphology, surface structure, crystal growth, dissolution, bond valence.

SOMMAIRE

Nous prédisons la morphologie des faces de base des minéraux contenant des feuillets à polyèdres uranylés en considérant le déficit en valences de liaison des chaînes de polyèdres, le décalage entre les feuillets, et l'agencement des complexes interstitiels entre les couches. Les unités structurales en feuillets de la schoepite, $[(UO_2)_8O_2(OH)_{12}](H_2O)_{12}$, et de la fourmariérite, $Pb[(UO_2)_4O_3(OH)_4](H_2O)_4$, possèdent la même topologie anionique de base. La stabilité de leurs bordures diffère en fonction du décalage de feuillets adjacents équivalent à une chaîne de polyèdres dans la schoepite, tandis que les feuillets adjacents ne sont pas décalés dans la fourmariérite. Les minéraux becquerelite, $^{[7]}Ca(H_2O)_4[(UO_2)_3O_2(OH)_3]_2\ (H_2O)_4$, compreignacite, $^{[7]}K_2(H_2O)_3\ [(UO_2)_3O_2(OH)_3]_2(H_2O)_4$, billietite, $^{[10]}Ba(H_2O)_4[(UO_2)_3O_2(OH)_3]_2\ (H_2O)_3$, protasite, $^{[10]}Ba(H_2O)_3[(UO_2)_3O_3(OH)_2]$, et masuyite, $^{[10]}Pb(H_2O)_3[(UO_2)_3O_3(OH)_2]$, possèdent tous des unités structurales ayant la même topologie anionique de base. La stabilité de la bordure de leurs feuillets diffère à cause des divers arrangements des espèces interstitielles. Dans la becquerelite, les cations interstitiels sont agencés en rangées parallèles à [010], tandis que dans la billietite et la compreignacite, les cations interstitiels

§ *Current address*: Department of Geological Sciences, University of Manitoba, Winnipeg, Manitoba R3T 2N2, Canada.
E-mail address: mschindl@lakeheadu.ca

sont agencés en rangées parallèles à [100]. Dans le cas de la masuyite et la protasite, la stabilité de leurs bordures dépendrait des différences majeures des déficits en valences de liaison des chaînes de polyèdres ayant des terminaisons gauche et droite. La stabilité des bordures des feuillets de la curite, $Pb_3[(UO_2)_8O_8(OH)_6](H_2O)_3$, est régie par le faible déficit en valences de liaison associé aux chaînes de polyèdres parallèles à [001] et [011], et par l'agencement des cations en rangées parallèles à [001]. Les minéraux du groupe de la carnotite contiennent l'unité structurale $[(UO_2)_2(V_2O_8)]^{2-}$, et la stabilité de la bordure de leurs feuillets dépendrait du faible déficit en valences de liaison des chaînes de polyèdres parallèles à [010] et [110]. Les minéraux du groupe de l'uranophane contiennent le feuillet $[(UO_2)SiO_3(OH)]^-$, et la stabilité de la bordure de leurs feuillets est plus fortement affectée par le déficit en valences de liaison des chaînes de polyèdres que par l'agencement des cations interstitiels, et par le décalage des feuillets. Toutes nos prédictions sont comparées avec la morphologie correspondante de cristaux étudiés par microscopie en force atomique (AFM), des images de cristaux disponibles, et des dessins de cristaux tirés surtout de la littérature plus ancienne. Toutes nos prédictions s'avèrent concordantes avec la morphologie observée de la face de base de ces minéraux.

Mots-clés: minéraux d'uranyle, morphologie, structure de surface, croissance cristalline, dissolution, valences de liaison.

Introduction

Uranyl-oxide minerals are common at many oxidized uranium deposits, and play a key role in the paragenesis of minerals that form where uraninite has been exposed to oxidizing meteoric water (Frondel 1958, Deliens 1977, Finch *et al.* 1992, Finch & Ewing 1992, Finch & Murakami 1999). Uranyl minerals have also been identified as corrosion products of UO_2 and spent nuclear fuel (Wadsen 1977, Wang & Katayama 1982, Forsyth & Werme 1992, Sunder *et al.* 1992, Wronkiewicz *et al.* 1992, 1996, Buck *et al.* 1997, 1998). Recently, the formation of schoepite, $[(UO_2)_8O_2(OH)_{12}](H_2O)_{12}$ has been observed on used depleted-uranium ammunition in Kosovo (United Nations Environmental Program 2001).

Chemical reactions on the surfaces of uranyl-sheet minerals are an important issue, as they result in the release of $(UO_2)^{2+}$ to natural waters. Therefore, a detailed atomic-scale understanding of the surface chemistry of uranyl-sheet minerals is desirable. Uranyl-sheet minerals contain layers of polymerized uranyl-polyhedra with uranium in [6], [7] and [8] coordination as tetragonal, pentagonal and hexagonal bipyramids, respectively. In these polyhedra, strong U–O uranyl bonds are not involved in linkage between uranyl polyhedra; they extend orthogonal to the sheet, whereas weaker equatorial U–φ bonds link the polyhedra in the plane of the sheet [φ: O^{2-}, $(OH)^-$, (H_2O)]. The equatorial O-atoms in the sheet of polyhedra can participate in acid–base reactions through protonation and deprotonation. Hence, edge surfaces on uranyl minerals are much more reactive than the corresponding basal surfaces because equatorial O-atoms on the edge surface almost always bond to fewer U^{6+} atoms than oxygen atoms in the sheet, and hence must satisfy their individual bond-valence requirements through a higher degree of protonation.

The Periodic Bond-Chain (PBC) theory (Hartman & Perdok 1955a, b, c) defines the basal face parallel to the sheets of uranyl polyhedra as an F face (flat face) because the sheet contains more than one periodic bond-chain. A PBC is an uninterrupted chain of strong bonds between building units. The basal face slowly grows, and therefore dominates the morphology of sheet-structure uranyl-oxide minerals. The morphology of the basal face itself is controlled by the faster-growing S faces (step faces), which contain only one type of periodic bond-chain.

Schindler *et al.* (2004a) showed that these periodic bond-chains can be represented by polyhedron chains in the sheet structural units of uranyl-oxide minerals. Parallel chains of polyhedra in the translation unit perpendicular to the basal face define the surface of an *edge*. The interaction of the surface of an edge with the aqueous species controls surface processes such as crystal growth and dissolution. These interactions depend on the surface structure of an edge, the pH value and the saturation index with respect to the mineral. Schindler *et al.* (2004a) also showed that the surface structure of an edge is characterized by the bond-valence deficiency of anion terminations along chains of polyhedra parallel to the edge, and by the shift and orientation of adjacent layers. Furthermore, they showed that the stability of edges also depends on the arrangement of the interstitial cations between the layers. In this paper, we will use this approach to predict the morphology of the basal faces of uranyl-oxide minerals, and will compare our predictions with AFM observations on synthetic crystals and morphological observations on natural crystals of uranyl-oxide minerals.

Experimental

Crystal growth, atomic-force microscopy and X-ray powder diffraction

In order to increase the database on the morphology of basal faces of uranyl-oxide crystals, we examined the crystal growth of uranyl-oxide minerals on the (001) face of dehydrated schoepite with an atomic-force microscope. The crystals of dehydrated schoepite were synthesized according to the procedure of Schindler *et al.* (2004a). After synthesis, 0.1 g of crystals were washed and brought in contact with 0.25 mol L^{-1} $BaCl_2$, KCl and $PbNO_3$ salt solutions at 25°C for 24 h. The

(001) face of the schoepite crystals was examined with the atomic force microscope (Digital Instruments Nanoscope III, Dimensional 3000). The surface was scanned in contact mode, and the images were analyzed with the Nanoscope Software package. The samples were subsequently examined by X-ray powder diffraction (Philips PW3040 powder diffractometer with Cu$K\alpha$ X-radiation) in order to identify the phases grown on the crystals of dehdyrated schoepite.

Collection of morphology data of basal faces of uranyl-oxide minerals

In order to determine the occurrence of edges on schoepite crystals and other uranyl-sheet minerals, we have examined images of crystals recorded by atomic force microscopy (AFM), or images (both photographs and sketches) drawn from the (mainly older) mineralogical literature. For the literature data, the indices of edges or the corresponding faces were determined by optical goniometry. In the case of AFM and images from Perloff (1998) and the internet, we indexed the edges by measuring the angles between the edges on the image and comparing them with corresponding angles derived from structural data.

The (001) Face of Schoepite

In schoepite, $[(UO_2)_8O_2(OH)_{12}](H_2O)_{12}$, there are eight crystallographically distinct sites occupied by U^{6+}, two of which are [7]-coordinated by two apical uranyl O-atoms and five equatorial (OH) groups, and six of which are [7]-coordinated by two apical uranyl O-atoms, one equatorial O-atom and four equatorial (OH)-groups (Finch *et al.* 1996). Schoepite has space-group symmetry $P2_1ca$ (orthorhombic), with a 14.337, b 16.813, c 14.731 Å. Figure 1 shows part of a (001) layer in schoepite, in which the pentagonal bipyramidal poly-

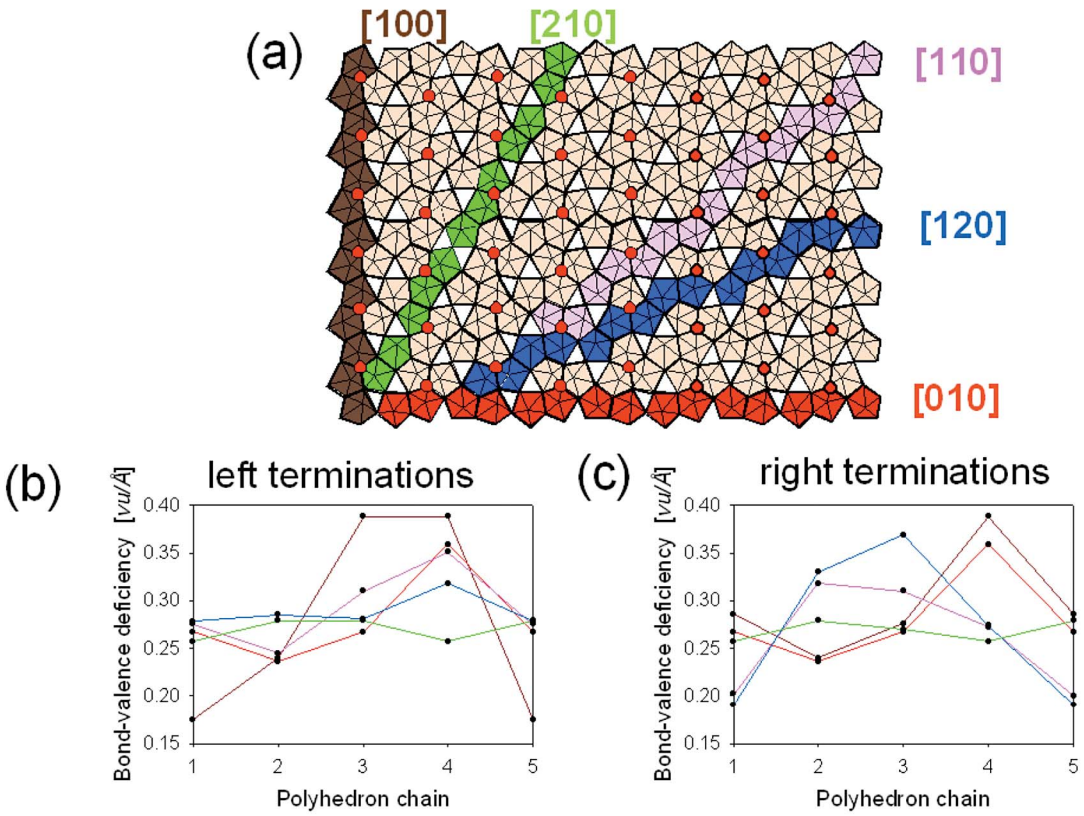

FIG. 1. (a) Polyhedron representation of the uranyl-oxide hydroxy-hydrate sheet in schoepite, $[(UO_2)_8O_2(OH)_{12}](H_2O)_{12}$; chains of polyhedra parallel to [100], [010], [120], [110] and [210] are shown in dark brown, red, blue, violet and blue-green, respectively. Equatorial O^{2-} anions of the uranyl polyhedra are shown as red-brown octagons, equatorial edges are shown as heavy black lines. (b), (c) Calculated bond-valence deficiencies for left and right anion-terminations on chains parallel to the [100], [010], [120], [110] and [210] edges in the uranyl sheet of schoepite. Bond valences were calculated using the curves of Brown & Altermatt (1985). The colors of the plots correspond to the colors of the different [*hk*0] directions in the schoepite sheet.

hedra share edges involving equatorial O- and (OH)-anions. The additional (H_2O) groups occur between the layers and link them together with weak hydrogen bonds.

Bond-valence deficiencies of chains of polyhedra in schoepite

Figure 1a shows selected chains of polyhedra parallel to [100], [010], [110], [120] and [210] in the schoepite sheet. Figures 1b and c show the change in bond-valence deficiency for the different chains. It is apparent that chains parallel to [100], [010], [110] and [120] have lower bond-valence deficiencies than chains parallel to [210]. The bond-valence deficiencies of the chains parallel to [210] are invariably high, whereas chains parallel to [100], [010], [110] and [120] have both low and high bond-valence deficiencies. Chains with low bond-valence deficiencies result in a low concentration of activated sites on the corresponding edges.

Orientation and shift of layers

Finch *et al.* (1996) showed that the positions of U^{6+} atoms and equatorial O-atoms in the structure of schoepite obey space-group symmetry *Pbca*. Adjacent layers are therefore related *via* a pseudo-two-fold screw axis parallel to [001]. Hence, right and left terminations of each chain of polyhedra occur on the same edge.

There is a shift between the layers parallel to the edges [100], [120], [110] and [210]. At those edges, therefore, chains of polyhedra of low bond-valence deficiency are parallel to chains of polyhedra with high bond-valence deficiency. For example, the chain of polyhedra parallel to [100] with the lowest minimum in bond-valence deficiency, 0.174 *vu* / Å, is parallel to a chain of polyhedra with a minimum in bond-valence deficiency of 0.276 *vu* / Å. Both chains could define an edge without an additional kink-site, but the large deficiency of one of the chains of polyhedra will produce a higher number of activated sites during crystal growth. This results in a higher growth-rate perpendicular to the chain of polyhedra, which produces a kink site (Schindler & Hawthorne 2004) between the adjacent layers on the [100] edge. Schindler *et al.* (2004a, Figs. 7a, b, c) predicted that this type of arrangement is less stable than an arrangement with chains of polyhedra of similar bond-valence deficiency along an edge. This is the case for adjacent layers (with no kink site) at the edge parallel to [010] (Schindler *et al.* 2004a, Fig. 7b); each layer is terminated by a chain of polyhedra with a bond-valence deficiency of 0.236 *vu*.

We are now able to predict the growth or dissolution rates of the different edges: they increase in the sequence [010] << [100] < [120] = [110] << [210], where "<" indicates a higher rate of growth of the corresponding edge. We predict that the edges [010] and [100] should invariably occur, independent of ΔpH and $\Delta\beta$, whereas the occurrence of the edges [120] and [110] depends on ΔpH and $\Delta\beta$, and the [210] edge should never occur.

Morphology of schoepite crystals

Figure 2a shows an AFM image of a schoepite crystal grown on the (104) surface of calcite (Schindler & Putnis 2004, who described in detail the relations between morphology and conditions of crystallization). The corresponding indices of the edges in the image are [120], [110], [100] and [010]. Figure 2b is an AFM image of schoepite crystals where the (001) face is defined by the [100] and [010] edges. Figure 2c shows a schoepite crystal from Katanga, Democratic Republic of Congo, with a prominent (001) face slightly elongate along [010] (http://www.trinityminerals.com/sm/uranium.shtml). The edges defining the (001) face have indices [120], [110], [100] and [010]. Figure 2d shows a drawing of a prismatic crystal of schoepite from Katanga on which the [100], [010] and [110] edges define the (001) face, and [120] edges occur between the (210) and (211) faces (indicated as m and P, respectively, in Fig. 2d; Walker 1923). Figure 2e shows typical rectangular crystals of schoepite from Katanga (http://webmineral.com/data/schoepite.shtml). The morphology of their (001) face is characterized primarily by [100] and [010] edges and, to a lesser extent, by the [110] edge (Palache 1934, Palache *et al.* 1944). These crystals are nearly identical to crystals grown under basic conditions (Fig. 2b, Schindler & Putnis 2004). Hence, they may have grown in a solution at low supersaturation and large differences between pH and pH_{pzc} (the pH of a solution in which a surface has zero net proton-charge: Stumm 1992, p. 18). These examples show that the morphology of schoepite crystals from growth experiments and from mineral samples are in good agreement with our predictions.

The (001) Face of Fourmarierite

Fourmarierite, $Pb[(UO_2)_4O_3(OH)_4](H_2O)_4$, has space-group symmetry $Bb2_1m$ (orthorhombic) with *a* 13.986, *b* 16.400, *c* 14.293 Å (Piret 1985). The uranyl sheet in fourmarierite has the composition $[(UO_2)_4O_3(OH)_4]^{2-}$, and its topology is identical to the topology of the uranyl sheet in schoepite (Burns 1999). The Pb^{2+} cations and (H_2O) groups occur between the uranyl sheets.

Figure 3a shows details of the uranyl sheet in fourmarierite. The equatorial O^{2-} ions are shown as black and red circles; the latter circles are identical to the O^{2-} positions in the schoepite sheet. However, in contrast to schoepite, there is no shift between the layers of polymerized uranyl-polyhedra in fourmarierite. However, adjacent layers are rotated by 180° to each other, which means that left and right terminations of the polyhedron chains occur on one edge. The interstitial cations are homogeneously distributed between

these layers and are not arranged in specific rows parallel an edge, such as in becquerelite and billietite (see Schindler *et al.* 2004a). Thus, the stability of edges should depend only on their individual bond-valence deficiencies and not on the arrangement of the layers or the distribution of cations in the interstices. Calculation of bond-valence deficiencies on chains of polyhedra in schoepite shows that the deficiency along each chain strongly depends on the number of O^{2-} anions. Inspection of the O^{2-} sites in the fourmarierite sheet shows that O^{2-} anion terminations occur on all chains parallel to [010], but not on all chains parallel to [100]. As a result, we expect that chains of polyhedra parallel to [100] have lower minima of bond-valence deficiency than chains parallel to [010]. This is indeed the case: the calculated bond-valence deficiencies for chains of polyhedra parallel to [100], [010], [120], [120] and [110] clearly show that the chain parallel to [100] has the lowest minimum in bond-valence deficiency (Fig. 3, right and left terminations). There are small differences between minima in bond-valence deficiency of chains parallel to [120] and [110]. Thus, we predict the probability of occurrence of edges to be [100] > [110] = [120] > [210] > [010]. This means that the (001) face of fourmarierite crystals grown in a solution close to equilibrium and at a pH close to the pH_{pzc} of the edges might be defined by the [100], [110], [120] and [210] edges. In a solution with a higher supersaturation with respect to fourmarierite and with a pH very different from the pH_{pzc}, we would expect elongate crystals parallel to

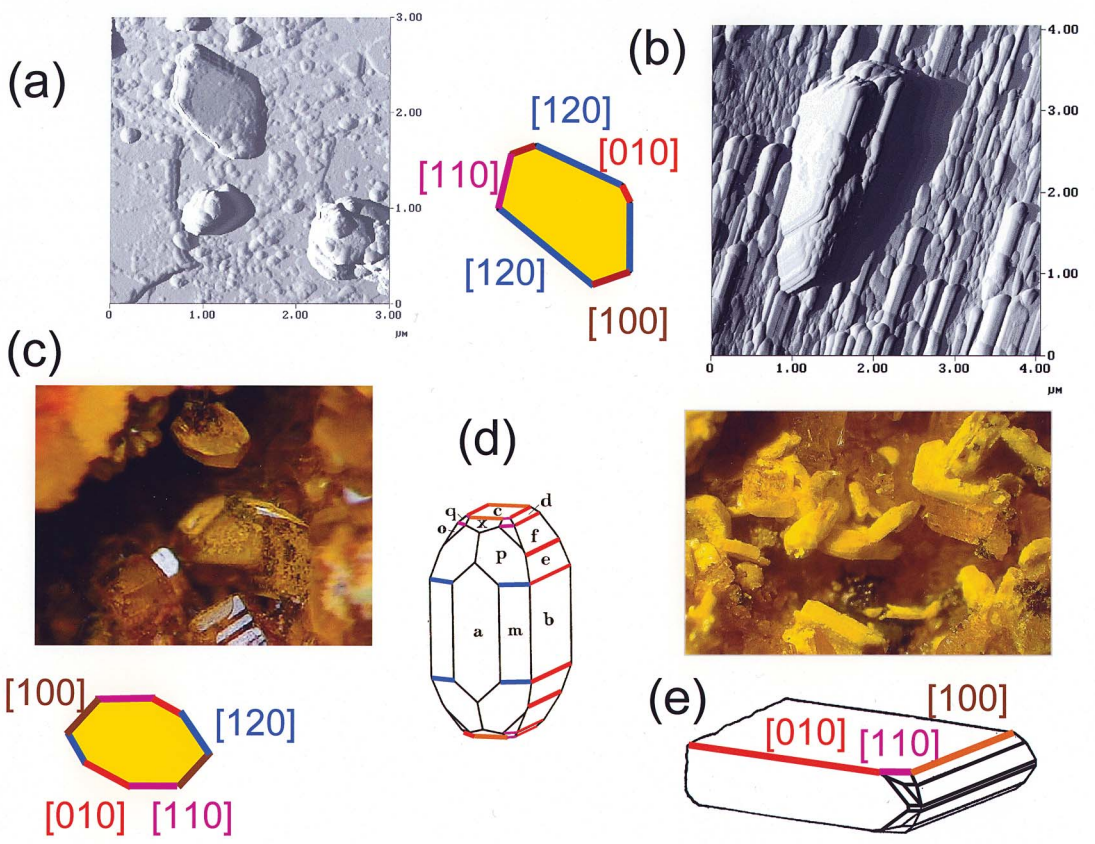

FIG. 2. (a) AFM image of a schoepite crystal grown in a weak acidic solution on the calcite (104) surface; the (001) face is defined by the [120], [110], [100] and [010] edges. (b) AFM image of schoepite crystals formed in a weak basic solution on the (104) surface of a calcite; their morphology is similar to that of crystals from Kasolo, Katanga, Democratic Republic of Congo (Walker 1923, Palache 1934). (c) Schoepite crystals with a prominent (001) face defined by the [120], [110], [100] and [010] edges (Perloff 1998). (d) Prismatic crystals of schoepite with a (001) face defined by [100], [010] and [110] edges; [120] edges occur between the (210) and (211) faces [indicated as (m) and P]. (e) Schoepite crystals from Kasolo, Democratic republic of Congo (Perloff 1998), together with a sketch of a crystal showing a dominant (001) face with [100], [010] and minor [110] edges (Palache *et al.* 1944).

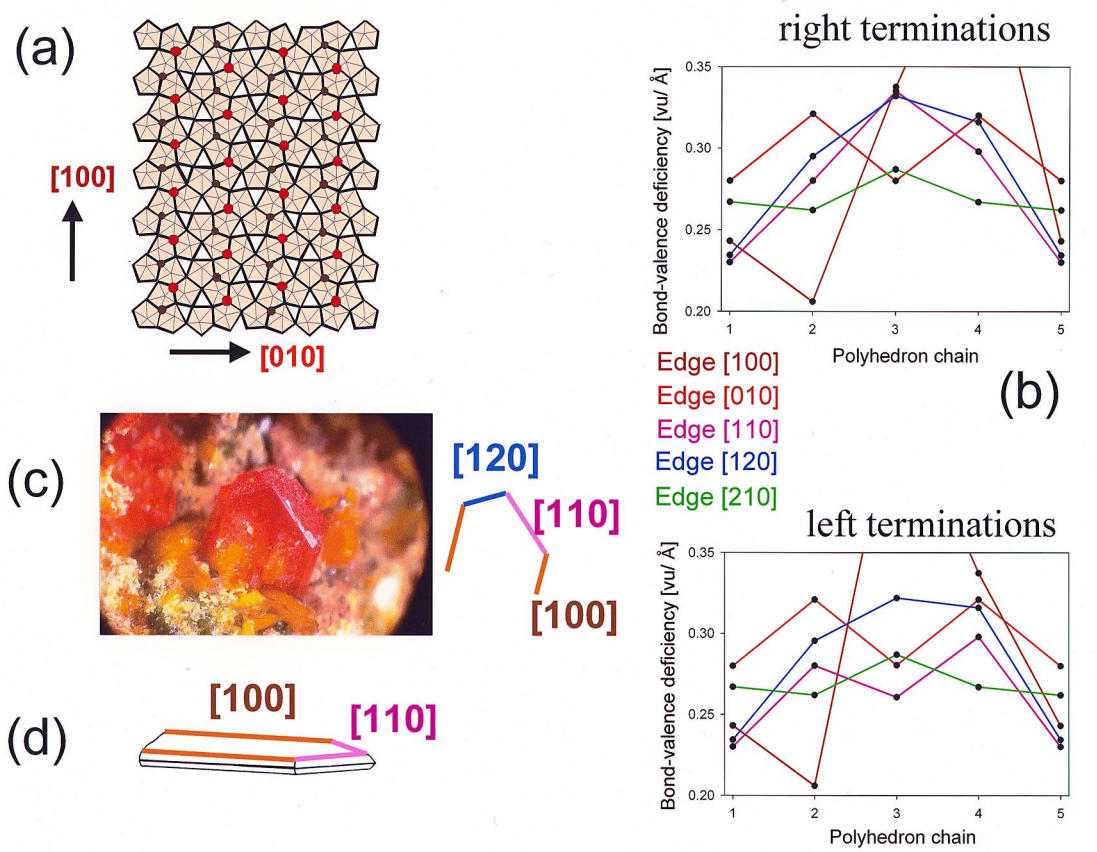

FIG. 3. (a) The $[(UO_2)_4O_3(OH)_4]^{2-}$ sheet as the structural unit in fourmarierite; the equatorial O^{2-} anions are identical to those in the analogous positions in the schoepite sheet and are shown as red circles, whereas the anions unique to fourmarierite are shown as brown circles. (b) Calculated bond-valence deficiencies of the right- and left-form chain-terminations on chains parallel to the [100], [010], [210], [110] and [120] edges. (c) A thick tabular orange crystal of fourmarierite from the Shinkolobwe mine, Democratic Republic of Congo (Perloff 1998), with a (001) face defined by the [100], [110] and [120] edges. (d) Morphology of fourmarierite crystals from Katanga, Democratic Republic of Congo, with a (001) face defined by [100] and [110] edges.

[100], and with a prominent (001) face that is defined only by the [100] and [110] or [120] edges.

Morphology of fourmarierite crystals

Figure 3c shows a thick tabular orange crystal of fourmarierite from the Shinkolobwe mine, Democratic Republic of Congo (Perloff 1998). Its (001) face is bounded mainly by the [100], [110] and [120] edges. Buttgenbach (1924) examined the morphology of fourmarierite crystals from Katanga, Democratic Republic of Congo, and described the crystals as elongate on [100], with dominant (001), (110) and (111) faces (based on the orientation of Piret 1985) (Fig. 3d). The (001) face in fourmarierite is bounded by the [100] and [110] edges, in good agreement with our predictions.

THE (001) FACE OF MINERALS OF THE BECQUERELITE GROUP

Minerals of the becquerelite group are becquerelite, $^{[7]}Ca(H_2O)_4[(UO_2)_3O_2(OH)_3]_2(H_2O)_4$, compreignacite, $^{[7]}K_2(H_2O)_3\ [(UO_2)_3O_2(OH)_3]_2(H_2O)_4$, billietite, $^{[10]}Ba(H_2O)_4[(UO_2)_3O_2(OH)_3]_2\ (H_2O)_3$, $^{[8]}K_2(^{[9]}Ca,Sr)(H_2O)_5[(UO_2)_3O_3(OH)_2]_2$, and rameauite, $K_2Ca[(UO_2)_6O_4(OH)_6]\ (H_2O)_6$. The chemical composition of their (sheet) structural unit is $[(UO_2)_3O_2(OH)_3]^-$, in which U^{6+} occurs in [7]-coordination (Fig. 4a). The topology of the sheet differs from that of sheets in fourmarierite and schoepite. The structures of becquerelite, compreignacite and billietite have orthorhombic symmetry, but the space-group symmetry and unit-cell dimensions vary with the type of interstitial cation and the number

of interstitial (H_2O) groups. We calculated the bond-valence deficiencies of the different chain-terminations of unit length *a* 13.8378 / 2 = 6.919, *b* 12.3781 Å from the crystal-structure data on becquerelite (Pagoaga *et al.* 1987), and will describe the crystal morphologies of becquerelite, billietite and compreignacite crystals on the basis of these cell dimensions and in the orientation given in Figure 4a.

In becquerelite, billietite and compreignacite, adjacent layers are rotated by 180° relative to each other. Hence, the left and right terminations of the same type of chain define the corresponding edges of two adjacent layers.

Interstitial complexes in becquerelite and billietite are arranged in rows parallel to [010] and [100], respectively. The corresponding crystals of both minerals are elongate in these directions. In compreignacite, the interstitial complexes are arranged in rows parallel to [100], and the interstitial K is highly disordered in those complexes (Burns 1998). Thus, we would expect similar morphologies for the (001) face in billietite and compreignacite.

Figure 4b shows the calculated bond-valence deficiencies of the chain terminations of the different chains of the uranyl sheet. It is apparent that the [110] and [100] edges contain chains with the lowest minima in bond-valence deficiency, and that the differences in minima are very small for chains parallel to [010], [210], [310] and [130]. Considering only the bond-valence deficiencies and not the arrangement of the interstitial species, we predict that the probability of occurrence of edges decreases in the sequence [110] = [100] >> [310] = [210] > [110] = [130].

Morphology of becquerelite, billietite and compreignacite

Figures 5a and 5b show an image of becquerelite crystals from Shinkolobwe, Democratic Republic of Congo (Perloff 1998) and the indices of the correspond-

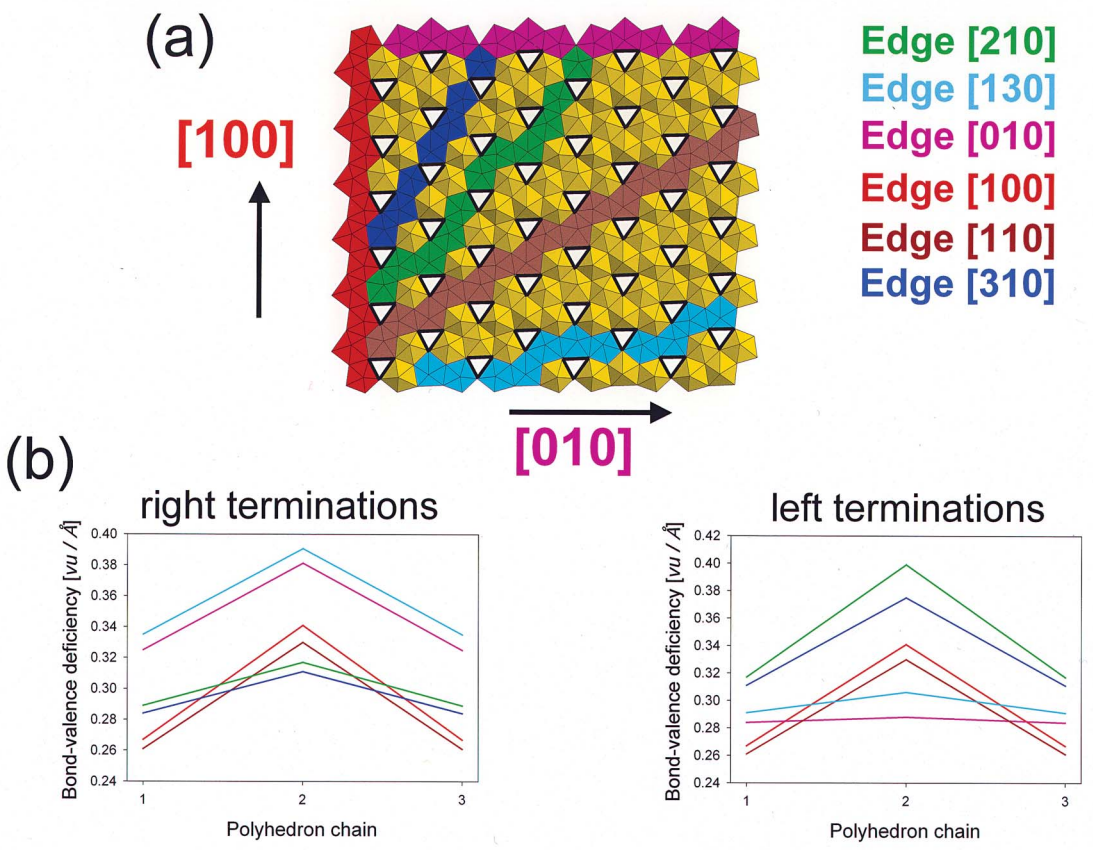

FIG. 4. (a) The $[(UO_2)_3O_2(OH)_3]_2^{2-}$ sheet as the structural unit in minerals of the becquerelite group. (b) Calculated bond-valence deficiencies of the left and right forms of chain terminations on chains parallel to the edges [100], [010], [310], [110], [130] and [210]. The positions of the (OH) groups are shown as vertices of a black triangle (Fig. 5a), and the chains parallel to the edges are indicated in the same colors as in Figure 4b.

ing edges: [110], [100] and [010]. Figures 5c and 5d show AFM images of becquerelite crystals grown on the (104) surface of calcite (Schindler *et al.* 2004b). Figure 5c shows an aggregate of small crystals of becquerelite grown in uranyl acetate + $NaCO_3$ solution for one month at a pH of 7.5–8.5. Figure 5d shows a parallel aggregate of larger crystals of becquerelite crystals in uranyl acetate solution at 100°C for 3 days at a pH of 5–6. In both cases, the indices of the edges are [110], [100] and [010] (Fig. 5e).

Figures 5f shows a crystal of billietite from Shinkolobwe, Democratic Republic of Congo (http://trinityminerals.com/sm2001/uranium.shtml); the indices of the edges present are [100], [010] and [110] (Fig. 5h). Figure 5g shows an AFM image of billietite crystals on the (001) surface of dehydrated schoepite; these crystals may be twinned on [110] (Fig. 5i). Twinning of billietite crystals is common on [111] and [110]; the latter twinning is particularly common and produces pseudohexagonal crystals (Schoep & Stradiot 1948; Fig. 5i).

Compreignacite was described in the same orientation as billietite. Protas (1964) reported equant crystals on which the (001) face is bounded by [100], [010], [110] and [310] edges (Fig. 5j). He also reported compreignacite crystals twinned on [110], for which the (001) face is not bounded by the [100] or [110] edges (Fig. 5k). The [100] and [110] edges, which are defined

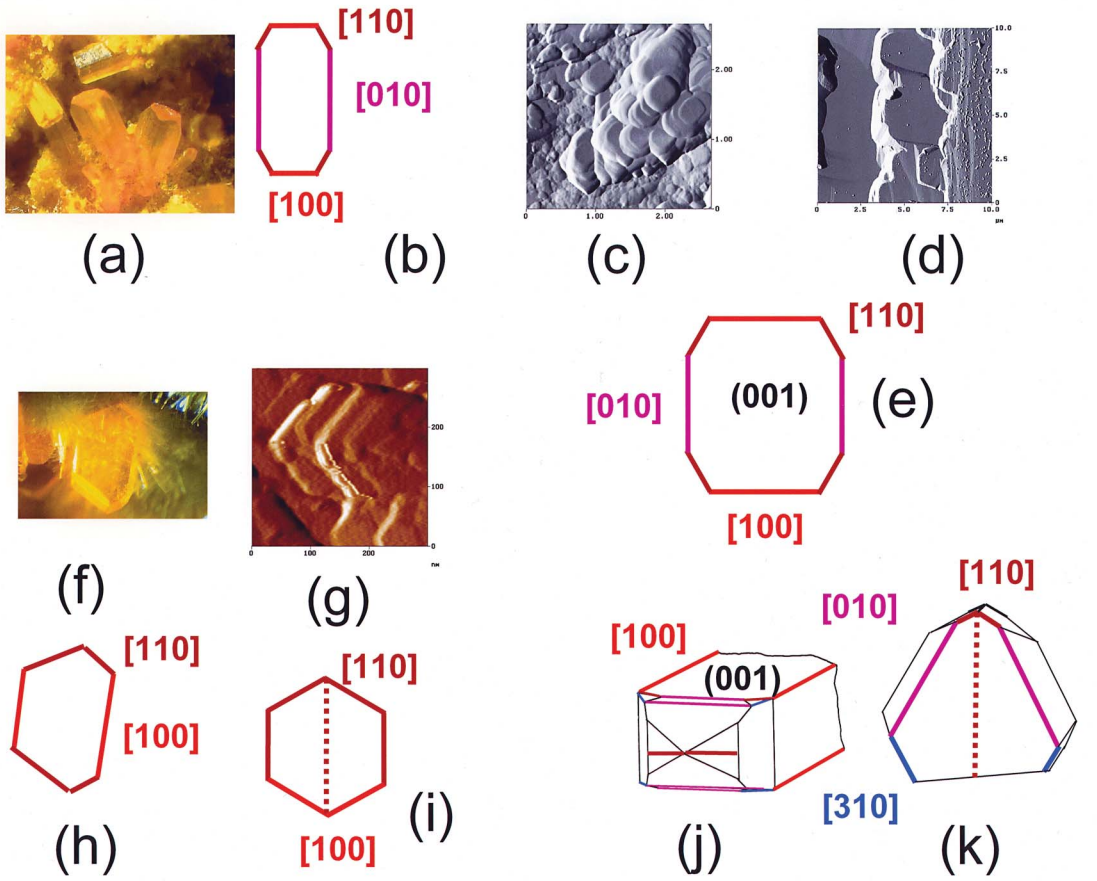

FIG. 5. (a, b) Crystals of becquerelite from Shinkolobwe, Democratic Republic of Congo (Perloff 1998) with a (001) face defined by the [110], [100] and [010] edges. (c, d) AFM images and (e) sketch of becquerelite crystals grown on the calcite (104) surface with (001) faces defined by the [110], [100] and [010] edges. (f) Crystal of billietite from Shinkolobwe, Democratic Republic of Congo (Perloff 1998) and (h) the corresponding sketch of the (001) face defined by the [100] and [110] edges. (g) AFM image of billietite crystals on the (001) surface of dehydrated schoepite. (i) Sketch of a crystal twinned by reflection on (110), with a (001) face defined by the [100] and [110] edges. (j) Bulky crystals of compreignacite with a (001) face defined by the [100], [110], [310] and [010] edges. (k) Compreignacite crystals twinned by reflection on [110] with a (001) face defined by the [010] and [310] edges.

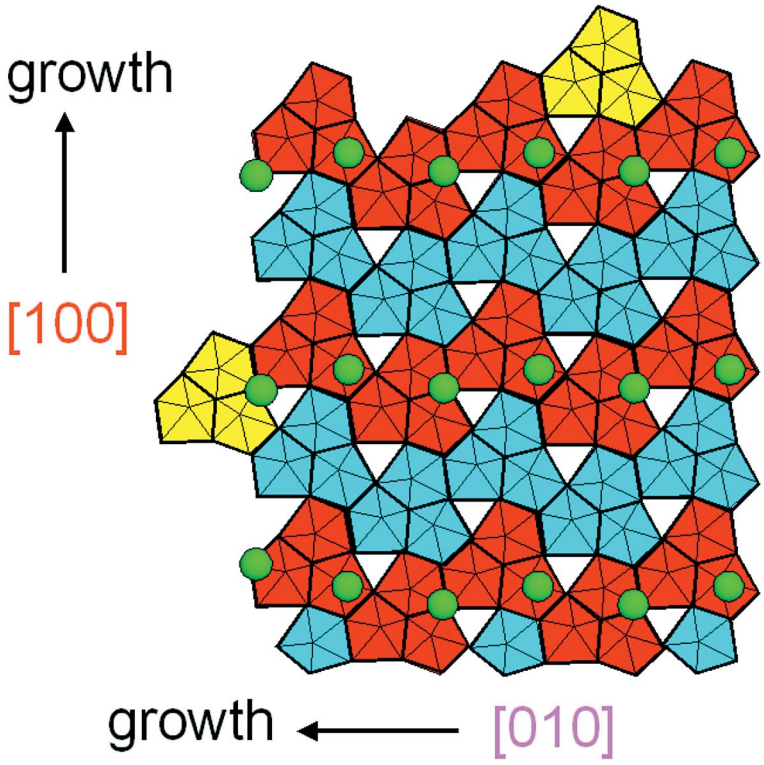

FIG. 6. The layer of polymerized uranyl-bearing polyhedra in becquerelite; this layer can be constructed of clusters of three polymerized pentagonal bipyramids (indicated in red and blue). These clusters are structurally identical to the principal aqueous species $[(UO_2)_3(OH)_5(H_2O)_5]^+$ in a weakly acidic solution. The position of the interstitial complex is indicated by the Ca atoms in the interlayer (green circles). Clusters attached on the [100] and [010] edges are indicated in yellow (see text for details).

by chains with the lowest bond-valence deficiencies, almost always occur on crystals of the becquerelite-group minerals. Except for twinned billietite and compreignacite, such crystals are elongate parallel to the rows of interstitial complexes in the interlayer. Hence, crystals of the becquerelite-group minerals grow parallel to the arrangement of interstitial complexes (which are only bonded to each other by weak hydrogen bonds). This is surprising, as it contradicts the basic ideas of PBC theory. One possible explanation of this phenomenon is illustrated in Figure 6, which shows the possible attachment of a cluster of three polymerized pentagonal bipyramids to the [010] and [100] edges in becquerelite [note that the (001) layer can be entirely constructed of such clusters]. Growth parallel to [100] corresponds to attachment of a cluster at the [010] edge. This attached cluster shares five ligands with the corresponding kink-site. If there is no layer above or below this layer, ligands (mainly O-atoms of the uranyl group) of the attached cluster do not receive bonds from the interstitial complex. If the cluster is attached to the [100] edge, there would be only four common ligands between cluster and kink site, but the ligands of the cluster would accept bonds from the interstitial complex.

THE (001) FACE OF MINERALS OF THE MASUYITE GROUP

The minerals of the masuyite group are protasite, $^{[10]}Ba(H_2O)_3[(UO_2)_3O_3(OH)_2]$, and masuyite, $^{[10]}Pb(H_2O)_3[(UO_2)_3O_3(OH)_2]$. They both have the (sheet) structural unit $[(UO_2)_3O_3(OH)_2]^{2-}$, which has the same topology as the sheet in minerals of the becquerelite group (Burns 1999; Figs. 4a, 7a). Both structures have space-group symmetry *Pn* (monoclinic), and the bond-valence deficiency of the chain terminations are calculated for the masuyite sheet with *a* 12.241, *c* 6.983 Å (Burns & Hanchar 1999). Reorientation of the axes (*c* = *a*, *a* = *b*) results in edge indices identical to those in the minerals of the becquerelite group.

The (OH) positions in the masuyite sheet differ from those in the isochemical sheet of richetite, $^{[6]}M_x$ $^{<[8.4]>}$ $Pb_{8.57}(H_2O)_{24}[(UO_2)_{18}O_{18}(OH)_{12}](H_2O)_{17}$ (Burns 1999). Compared to the sheet in minerals of the becquerelite group, one of the three (OH) groups is missing (Figs. 4a, 7a). This results in loss of mirror planes through the triangles parallel to [110] and [100] (Fig. 7a). As a result, we expect a high variation in bond-valence deficiencies on the right and left terminations of chains parallel to [110] and [100]. This is indeed the case: the minima in bond-valence deficiencies are lower on the left termination than on the right termination (Fig. 7b). This indicates the highly anisotropic character of the corresponding edges during dissolution and crystal growth. There is no shift between the layers either in masuyite or protasite, and the interstitial complexes are more or less homogeneously distributed in the interlayer of both minerals (Burns & Hanchar 1999, Pagoaga *et al.* 1987). Thus we have to consider only the average minima in bond-valence deficiencies for both terminations. Based on these minima, we predict that the probability of occurrence of edges decreases in the sequence [110] > [100] >> [130] > [310] = [010] > [210].

Morphology of masuyite and protasite

Vaes (1947) and Pagoaga *et al.* (1987) observed sector twinning with a 60° rotation of the twin plane around [001] in masuyite and protasite; the corresponding twin planes are [100] and [110]. Figure 7c shows a twin on [110], where the (001) face is bounded by the [100] and [110] edges (Vaes 1947). These observations indicate that the twin planes occur parallel to the missing mirror planes orthogonal to [100] and [110]. Instead of the predicted anisotropic growth of crystals, masuyite and protasite crystals show extensive twinning on [100] and [110]. This extensive twinning may be a result of the

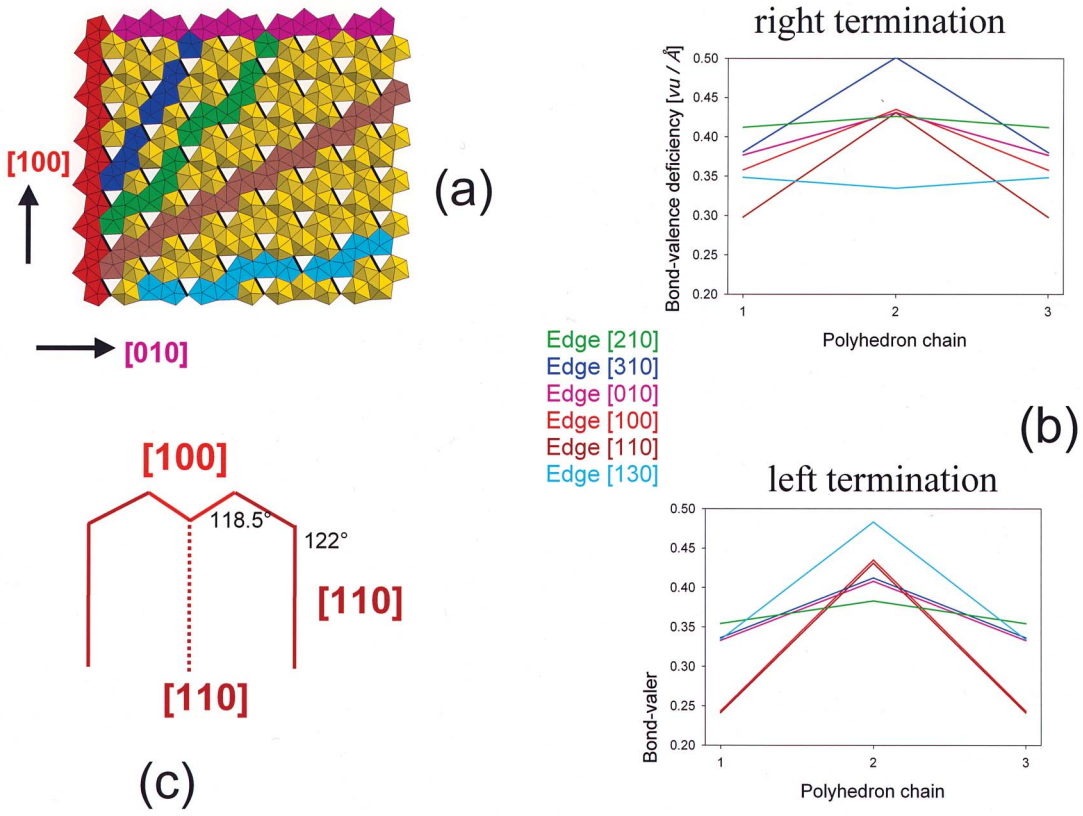

FIG. 7. (a) The $[(UO_2)_3O_3(OH)_2]^{2-}$ structural unit in minerals of the masuyite group. (b) Calculated bond-valence deficiencies of the left and right forms of chain terminations on chains parallel to the edges [100], [010], [310], [110], [130] and [210]. (c) Twins of masuyite (or protasite) crystals across [110], with the (001) face defined by the [100] and [110] edges.

large differences in the minima of the bond-valence deficiencies of the corresponding chains.

The (100) Face of Curite

Curite, $Pb_3[(UO_2)_8O_8(OH)_6](H_2O)_3$, has space-group symmetry *Pnam*, with *a* 12.551, *b* 13.003, *c* 8.390 Å (Taylor *et al.* 1981). The (sheet) structural unit is parallel to (100) and contains pentagonal and tetragonal biypramids. The arrangement of polyhedra produces slabs parallel to [001] that are linked *via* equatorial (OH) groups (Fig. 8a). In space-group symmetry *Pnam*, adjacent layers are related by a two-fold screw axis, and therefore are rotated by 180° relative to each other. Hence, left and right terminations of the chains of polyhedra occur together on the corresponding edges. The interstitial complexes are arranged in rows parallel to [001]. Similar to the minerals of the becquerelite group, an attached cluster or polyhedron at the [100] edge will accept bonds from the interstitial complex above or below the corresponding kink-site. Hence, the arrangement of interstitial complexes along [001] may promote growth in this direction. Figure 8b shows the calculated bond-valence deficiency for chains of polyhedra parallel to the edges [001], [012], [021], [011] and [010], where the [021] chain is a linear combination of the [001] and [011] chains, and the [012] chain is a combination of the [011] and [010] chains. There are many other possible chains that are a linear combination of either [001] and [011] or [010] and [011]. In the first case, we can indicate the chains with the general indices [0*k*>*l*], and in the second case with the general indices [0*k*<*l*]. On the basis of the bond-valence deficiencies of the chains of polyhedra parallel to [001], [011] and [010], one would expect that the chains of polyhedra parallel to [0*k*>*l*] have lower deficiencies than chains of polyhedra parallel to [0*k*<*l*]. This is indeed the case; chains of polyhedra parallel to [021] have a lower mini-

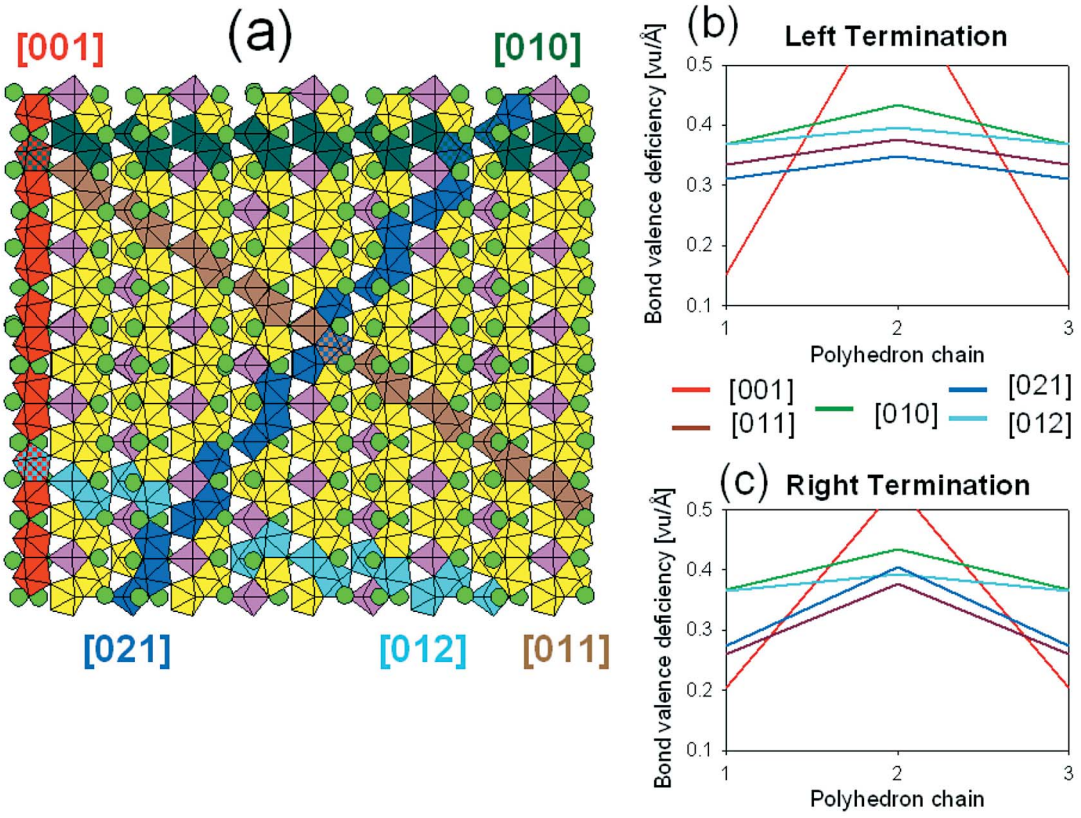

FIG. 8. (a) The $[(UO_2)_8O_8(OH)_6]^{2-}$ structural unit in curite and the chains of polyhedra parallel to [001] (red), [011] (brown), [010] (dark green), [021] (dark blue) and [012] (light blue). The positions of the Pb atoms are indicated with large green circles. (b) Calculated bond-valence deficiencies of the left and right forms of chain terminations on chains parallel to the edges [001], [010], [011], [012] and [021].

mum in bond-valence deficiency than chains of polyhedra parallel to [012] (Figs. 8b, c).

The minima in bond-valence deficiency of chain terminations in the right and left form indicate that the probability of occurrence of edges decreases in the sequence [001] > [011] = [0*k*>*l*] > [0*k*<*l*] > [010]. Because the minima in bond-valence deficiency indicate a high stability of the [001] edge and because the interstitial complexes are arranged parallel to this edge, we predict that the (001) face will be prominent on curite crystals, which will be dominated by the [001] edge.

Figures 9a, b show curite crystals obtained by synthesis (Schindler *et al.* in prep.) and from a mineral sample from the Shinkolobwe mine, Democratic Republic of Congo. Both crystals are elongate parallel to [001] (Perloff 1998), but the synthetic crystal is defined by [011] and [0*k*>*l*] edges (with $k = 4$ and $l = 3$), whereas the crystals of the mineral sample are exclusively defined by the [011] and [001] edges (Fig. 9d). Elongation of the crystals parallel to the [001] edge indicates the predicted dominance of that edge, and the occurrence of the [011] and [0*k*>*l*] edges also is in agreement with our predictions.

The (001) Face of Minerals of the Carnotite Group

The minerals of the carnotite group contain the structural unit $[(UO_2)_2(V_2O_8)]^{2-}$, a sheet containing (UO_7) pentagonal bipyramids and ($V^{5+}O_5$) square pyramids. The ($V^{5+}O_5$) square pyramids share common edges and form a [V_2O_8] dimer, which shares corners with dimers of edge-sharing (UO_7) pentagonal bipyramids (Fig. 10a).

Five-coordinated vanadium in ($V^{5+}O_5$) square pyramids is characterized by the occurrence of one or two strong vanadyl bonds. Schindler *et al.* (2000) indicated the number of vanadyl bonds by a three-part coordination number in which the number of bonds are listed in the order *vanadyl*, *equatorial* and *trans*. In the minerals of the carnotite group, V^{5+} is in [1+4] coordination (*i.e.*, there is one vanadyl bond, four equatorial bonds and no

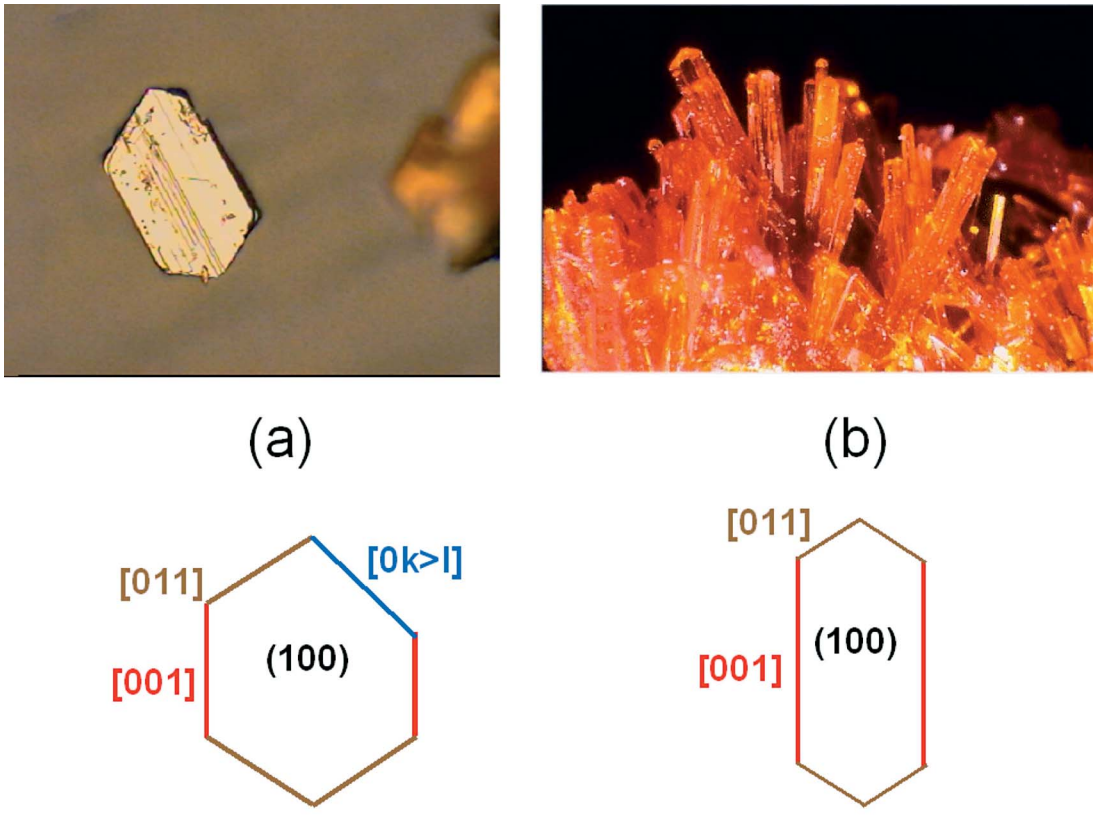

FIG. 9. (a) Synthetic crystal of curite, and (b) red crystals of curite from the Shinkolobwe mine, Democratic Republic of Congo (Perloff 1998), with a (100) face defined by [001], [0*k*>*l*] (with $k = 4$ and $l = 3$) and [011] edges.

trans bonds), and the average equatorial V^{5+}–O bond-valence is 0.79 *vu* (Schindler *et al.* 2000).

Depending on the interstitial complex, the minerals of the carnotite group have orthorhombic or monoclinic symmetry. Structural data of minerals of the carnotite group are available for francevillite (Mereiter 1986), curienite (Borène & Cesbron 1971), and sengierite (Piret *et al.* 1980). The structural data show that there are no shifts between the layers, and that the interstitial complexes are more or less equally distributed between the layers of these minerals. The bond-valence deficiencies of the different chain-terminations are calculated with the cell *a* 10.419, *b* 8.510 Å taken from the structure refinement of francevillite, $^{[9]}Ba(H_2O)_5[(UO_2)_2(V_2O_8)]$ (Mereiter 1986). Figure 10b shows the calculated bond-valence deficiencies of chain terminations parallel to several edges. Inspection of the corresponding minima in bond-valence deficiency shows that the probability of occurrence of edges decreases in the sequence [010] > [110] >> [100] = [120] > [210].

Morphology of minerals of the carnotite group

Minerals of the carnotite group form large idiomorphic crystals. Figure 10c shows green crystals of sengierite, $^{[6]}Cu_2(OH)_2(H_2O)_6[(UO_2)_2(V_2O_8)]$, from the Luiswishi mine, Democratic Republic of Congo (Perloff 1998) and yellow crystals of tyuyamunite, $Ca[(UO_2)_2(V_2O_8)](H_2O)_8$, from the Marie mine, Montana (http://www.dakotamatrix. com/GalleryImages/Rare/tyuy1b.jpg). Figure 10d shows the general morphology of the (001) basal face on almost all crystals of minerals of the carnotite group (Frondel 1958). The (001) face is bounded primarily by the [010] and [110] edges, with

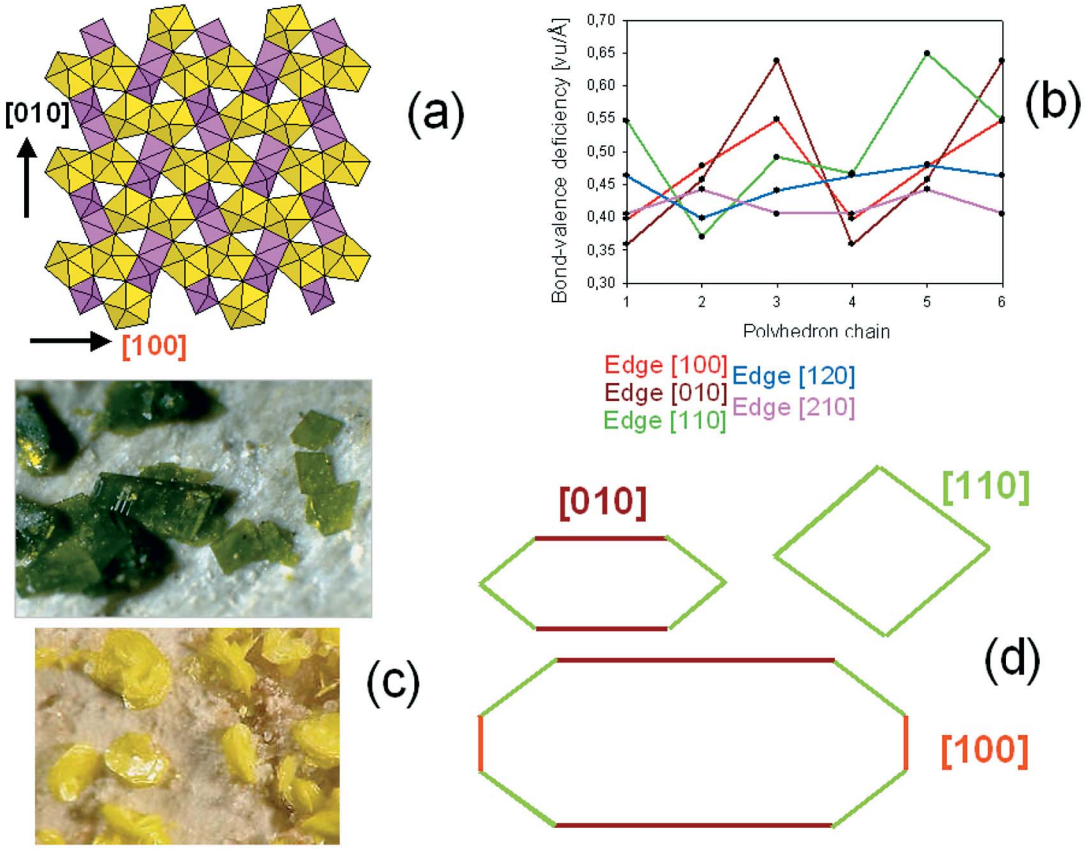

FIG. 10. (a) The $[(UO_2)_2(V_2O_8)]^{2-}$ structural unit in minerals of the carnotite group. (b) Calculated bond-valence deficiencies of chain terminations on chains parallel to the edges [100], [010], [110], [120] and [210]. (c) Green crystals of sengierite from the Luiswishi mine, Democratic Republic of Congo (Perloff 1998) and yellow crystals of tyuyamunite from the Marie mine, Montana (http://www.dakotamatrix.com/galleryimages/rare/tyuy1b.jpg). (d) Characteristic morphologies of the basal (001) face, with dominant [010] and [110] and minor [100] edges.

small [100] edges. These observations are in agreement with our predictions. The geometrical arrangement of interstitial cations is similar in all minerals of the carnotite group, and hence the different types of interstitial cations have minor or negligible effect on the stability of specific edges on the $[(UO_2)_2(V_2O_8)]^{2-}$ sheet.

The (010) Face of Minerals of the Uranophane Group

The minerals of the uranophane group are based on $[(UO_2)SiO_3(OH)]^-$ sheets, which contain $(U^{6+}\varphi_7)$ pentagonal bipyramids and acid $[SiO_3(OH)]$ groups (Fig. 11a). The pentagonal bipyramids share edges to form chains connected by $(Si\varphi_4)$ tetrahedra. The (OH) groups are located at the free apices of the $(Si\varphi_4)$ tetrahedra and form hydrogen bonds to interstitial (H_2O) groups. The minerals of the uranophane group are monoclinic and triclinic. The structural data on these minerals indicate that between the layers, there is a minimum shift that does not exceed one chain-width, and this small shift may not affect the stability of the corresponding edges. Interstitial complexes are homogeneously distributed between the layers in minerals with the α-uranophane structure-type (Burns 1999). For the β-uranophane structure, the interstitial complexes are arranged in rows parallel to [100] (Fig. 11a). Each interstitial complex occurs above and below the uranyl chain parallel to [001]. An attached pentagonal bipyramid on this chain will not accept any bonds from the interstitial complex. Hence, the interstitial complex cannot promote cluster attachment at the [001] edge, and the arrangement of interstitial cations in β-uranophane may not significantly influence growth of the crystals. The bond-valence deficiency of the chain terminations are calculated with the cell *a* 6.632, *c* 13.966 Å of β-uranophane (re-

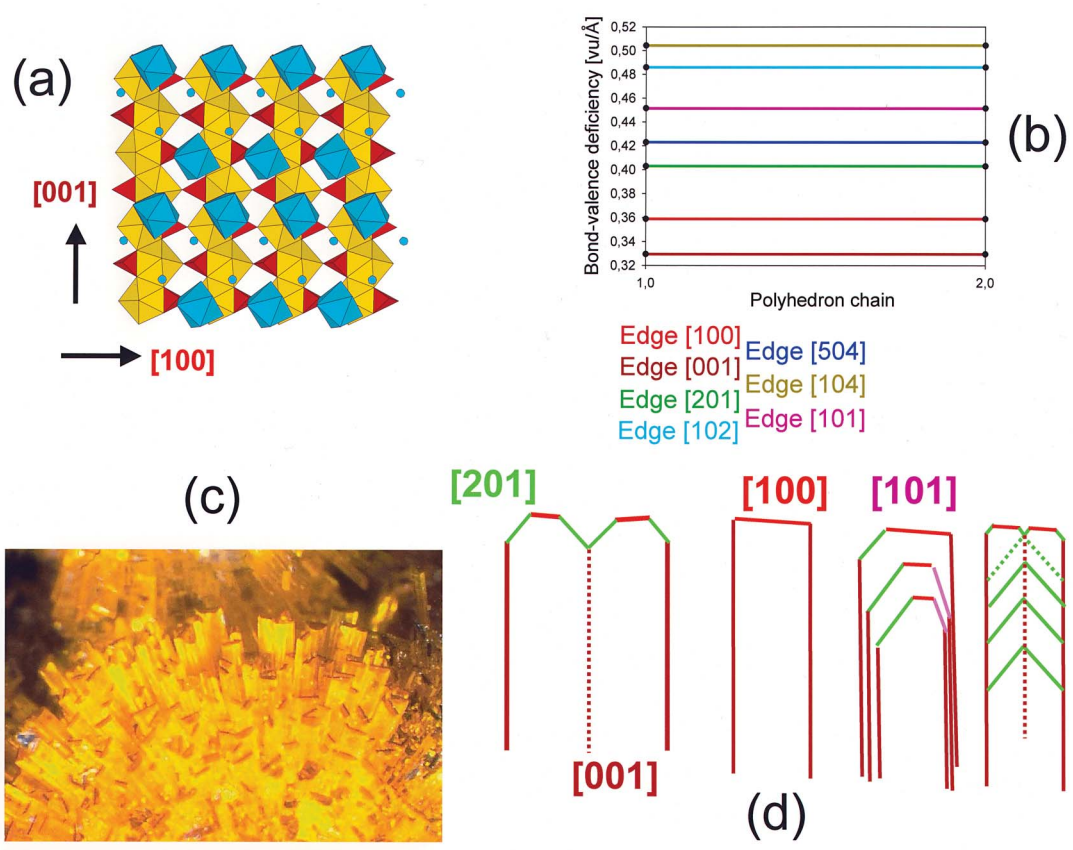

FIG. 11. The $[(UO_2)SiO_3(OH)]^-$ structural unit in minerals of the uranophane group, with the interstitial $(Ca\varphi_8)$ polyhedra indicated in light blue. (b) Calculated bond-valence deficiencies of chain terminations on chains parallel to the edges [001], [100], [201], [504], [101], [102] and [104]. (c) Yellow prisms of β-uranophane from the Rossing mine, Namibia (Perloff 1998). (d) Morphology of β-uranophane crystals with a (010) face defined by the [001] and [100] edges; the "edges" [201] and [101] occur mainly as growth zones.

oriented from *abc* to *cba*, Viswanathan & Harneit 1986) and with an average bond-valence of 1.0 *vu* for the equatorial Si–O bond. In $[(UO_2)SiO_3(OH)]^-$, if one considers chains of polyhedra that do not contain silicate tetrahedra with more than one free equatorial ligand, every [*h0l*] edge has only one possible chain-termination. Figure 11b shows the corresponding bond-valence deficiency of the single chain-termination parallel to each edge. The minima in deficiency indicate that the probability of the occurrence of edges decreases in the sequence [001] >> [100] >> [201] >> [504] >> [101] >> [102] >> [104].

Morphology of minerals of the uranophane group

All minerals of the uranophane group form prismatic to acicular crystals parallel to [001] and with a prominent (010) basal face. Figure 11c shows yellow prisms of β-uranophane, $^{[8]}Ca(H_2O)_5[(UO_2)(SiO_3OH)]_2$, from the Rossing mine, Namibia (Perloff 1998). Steinocher & Nováček (1939) and Branche *et al.* (1951) showed that the termination of β-uranophane crystals is bounded by the [100], [201] and [101] edges. The latter two edges occur mainly on growth zones, but almost disappear in the last stages of crystallization (Fig. 11d). These observations on β-uranophane show for the first time the direct relation between growth rate and bond-valence deficiency on the corresponding chains of polyhedra in uranyl-oxide minerals: the chain parallel to [100] has a lower minimum in bond-valence deficiency than the chains parallel to the faster-growing [201] and [101] edges. The observed morphology is thus in agreement with our predictions.

Summary

We can predict the occurrence of edges on the basal faces of uranyl-oxide minerals using the bond-valence deficiency of anion-terminations along chains of polyhedra, the shift and orientation of adjacent layers, and the arrangement of interstitial cations (Schindler & Hawthorne 2004). These predictions are in agreement with observation on minerals with different interstitial complexes and with different sheets as structural units.

Acknowledgements

We thank referees Mike Hochella and Cornelis Woensdregt and Editor Bob Martin for their comments, which added considerably to the clarity of this paper. MS thanks the Deutsche Forschungsgemeinschaft for an Emmy Noether Fellowshp. FCH was supported by a Canada Research Chair in Crystallography and Mineralogy and by a Discovery Grant from the Natural Sciences and Engineering Research Council of Canada.

References

Borène, J. & Cesbron, F. (1971): Structure cristalline de la curiénite, $Pb(UO_2)_2(VO_4)_2 \cdot 5H_2O$. *Bull. Soc. fr. Minéral. Cristallogr.* **94**, 8-14.

Branche, G., Chervet, J. & Guillemin, C. (1951): Nouvelles espèce uranifères françaises. *Bull. Soc. Fr. Minéral. Cristallogr* **74**, 457-488.

Brown, I.D. & Altermatt, D. (1985): Bond-valence parameters obtained from a systematic analysis of the inorganic crystal structure database. *Acta Crystallogr.* **B41**, 244-247.

Buck, E.C., Finch, R.J., Finn, P.A. & Bates, J.K. (1998): Np in dehydrated schoepite. In Scientific Basis for Nuclear Waste Management XXI (I.A. McKinley & C. McCombie, eds.). *Mater. Res. Soc. Proc.* **506**, 87-94.

_____, Wronkiewicz, D.J., Finn, P.A. & Bates, J.K. (1997): A new uranyl oxide hydrate phase derived from spent fuel alteration. *J. Nucl. Mater.* **249**, 70-76.

Burns, P.C. (1998): The structure of boltwoodite and implications for the solid-solution toward sodium boltwoodite. *Can. Mineral.* **36**, 1069-1075.

_____ (1999): The crystal chemistry of uranium. *In* Uranium: Mineralogy, Geochemistry and the Environment (P.C. Burns & R. Finch, eds.). *Rev. Mineral.* **38**, 23-90.

_____ & Hanchar, J.M. (1999): The structure of masuyite, $Pb[(UO_2)_3O_3(OH)_2](H_2O)_3$, and its relationship to protasite. *Can. Mineral.* **37**, 1483-1491.

Buttgenbach, H. (1924): La fourmariérite, nouvelle espèce minérale. *Ann. Soc. Géol. Belg.* **47**, 41.

Deliens, M. (1977): Associations de minéraux secondaires d'uranium à Shinkolobwe (région du Shaba, Zaïre). *Bull. Soc. fr. Minéral. Cristallogr.* **100**, 32-38.

Finch, R.J., Cooper, M.A., Hawthorne, F.C. & Ewing, R.C. (1996): The crystal structure of schoepite, $[(UO_2)_8O_2(OH)_{12}](H_2O)_{12}$. *Can. Mineral.* **34**, 1071-1088.

_____ & Ewing, R.C. (1992): The corrosion of uraninite under oxidizing conditions. *J. Nucl. Mater.* **190**, 133-156.

_____, Miller, M.L. & Ewing, R.C. (1992): Weathering of natural uranyl oxide hydrates: schoepite polytypes and dehydration effects. *Radiochim. Acta* **58/59**, 433-443.

_____ & Murakami, T. (1999): Systematics and paragenesis of uranium minerals. *In* Uranium: Mineralogy, Geochemistry and the Environment (P.C. Burns & R.J. Finch, eds.). *Rev. Mineral.* **38**, 91-179.

Forsyth, R.S. & Werme, L.O. (1992): Spent fuel corrosion and dissolution. *J. Nucl. Mater.* **190**, 3-19.

Frondel, C. (1958): Systematic mineralogy of uranium and thorium. *U.S. Geol. Surv., Bull.* **1064**.

HARTMAN, P. & PERDOK, W.G. (1955a): On the relations between structure and morphology of crystals I. *Acta Crystallogr.* **8**, 49-52.

_____ & _____ (1955b): On the relations between structure and morphology of crystals II. *Acta Crystallogr.* **8**, 521-524.

_____ & _____ (1955c): On the relations between structure and morphology of crystals III. *Acta Crystallogr.* **8**, 525-529.

MEREITER, K. (1986): Crystal structure refinements of two francevillites, (Ba,Pb)[$(UO_2)_2V_2O_8$]•$5H_2O$. *Neues Jahrb. Mineral., Monatsh.*, 552-560.

PAGOAGA, M.K., APPLEMAN, D.E. & STEWART, J.M. (1987): Crystal structures and crystal chemistry of the uranyl oxide hydrates becquerelite, billietite, and protasite. *Am. Mineral.* **72**, 1230-1238.

PALACHE, C. (1934): Crystallography of the uranium oxides. *Am. Mineral.* **19**, 309-315.

_____, BERMAN, H. & FRONDEL, C. (1944): *The System of Mineralogy*. **1**. *Elements, Sulfides, Sulfosalts, Oxides*. John Wiley and Sons, New York, N.Y. (p. 627).

PERLOFF, L. (1998): *The Photo Atlas of Minerals* (A.R. Kamp & G. Gerhold, eds.). The Gem and Mineral Council, Los Angeles County Museum of Natural History, Los Angeles, California.

PIRET, P. (1985): Structure cristalline de la fourmariérite, $Pb(UO_2)_4O_3(OH)_4$•$4H_2O$. *Bull. Minéral.* **108**, 659-665.

_____, DECLERCQ, J.-P. & WAUTERS-STOOP, D. (1980): Structure cristalline de la sengiérite. *Bull. Minéral.* **103**, 176-178.

PROTAS, J. (1964): Une nouvelle espèce minérale: la compreignacite, K_2O•$6UO_3$•$11H_2O$. *Bull. Minéral.* **87**, 365-371.

SCHINDLER, M. & HAWTHORNE, F.C. (2004): A bond-valence approach to uranyl oxysalt minerals. I. Crystal structure and chemical composition. *Can. Mineral.* **42**, 1601-1627.

_____, _____ & BAUR, W.H. (2000): Crystal-chemical aspects of vanadium: polyhedral geometries, characteristic bond-valences and polymerization of (VO_n) polyhedra. *Chem. Mater.* **12**, 1248-1259.

_____, _____, PUTNIS, C. & PUTNIS, A. (2004b): Growth of uranyl-hydroxy-hydrate and uranyl-carbonate minerals on the (104) calcite surface. *Can. Mineral.* **42**, 1683-1697.

_____, MUTTER, A. HAWTHORNE, F.C. & PUTNIS, A. (2004a): Prediction of crystal morphology of complex uranyl-sheet minerals. I. Theory. *Can. Mineral.* **42**, 1629-1649.

_____ & PUTNIS, A. (2004): Crystal growth of schoepite on the (104) surface of calcite. *Can. Mineral.* **42**, 1667-1681.

SCHOEP, A. & STRADIOT, S. (1948): Additional data on the properties of becquerelite and billietite. *Am. Mineral.* **33**, 503-507.

STEINOCHER, V. & NOVÁČEK, R. (1939): On β-uranotile. *Am. Mineral.* **24**, 324-338.

STUMM, W. (1992): *Chemistry of the Solid–Water Interface*. John Wiley & Sons, New York, N.Y. (p. 428).

SUNDER, S., SHOESMITH, D.W., CHRISTENSEN, H. & MILLER, N.H. (1992): Oxidation of UO_2 fuel by the products of gamma radiolysis of water. *J. Nucl. Mater.* **190**, 78-86.

TAYLOR, J.C., STUART, W.I. & MUMME, I.A. (1981): The crystal structure of curite. *J. Inorg. Nucl. Chem.* **43**, 2419-2423.

UNITED NATIONS ENVIRONMENT PROGRAM (2001): Depleted Uranium in Kosovo (2001). Post-conflict environmental assessment.

VAES, J.F. (1947): Six nouveaux minéraux d'urane provenant de Shinkolobwe (Katanga). *Ann. Soc. Géol. Belg.* **70**, 212-230.

VISWANATHAN, K. & HARNEIT, O. (1986): Refined crystal structure of β-uranophane $Ca(UO_2)_2(SiO_3OH)_2$•$5H_2O$. *Am. Mineral.* **71**, 1489-1493.

WADSEN, T. (1977): The oxidation of polycrystalline uranium dioxide in air at room temperature. *J. Nucl. Mater.* **64**, 315.

WALKER, T.L. (1923): Schoepite, a new uranium minerals from Kasolo, Belgian Congo. *Am. Mineral.* **8**, 67-69.

WANG, R. & KATAYAMA, J.B. (1982): Dissolution mechanism for UO_2, and spent fuel. *Nucl. Chem. Waste Management* **3**, 83-90.

WRONKIEWICZ, D.J., BATES, J.K. GERDING, T.J., VELECKIS, E. & TANI, B.S. (1992): Uranium release and secondary phase formation during unsaturated testing of UO_2 at 90°C. *J. Nucl. Mater.* **190**, 107-127.

_____, _____, WOLF, S.F. & BUCK, E.C. (1996): Ten year results from unsaturated drip tests with UO_2 at 90°C: implications for the corrosion of spent nuclear fuel. *J. Nucl. Mater.* **238**, 78-95.

Received August 12, 2003, revised manuscript accepted September 8, 2004.